

Study of $e^+e^- \rightarrow p\bar{p}\pi^0$ in the Vicinity of the $\psi(3770)$

M. Ablikim¹, M. N. Achasov^{8,a}, X. C. Ai¹, O. Albayrak⁴, M. Albrecht³, D. J. Ambrose⁴¹, F. F. An¹, Q. An⁴², J. Z. Bai¹, R. Baldini Ferroli^{19A}, Y. Ban²⁸, J. V. Bennett¹⁸, M. Bertani^{19A}, J. M. Bian⁴⁰, E. Boger^{21,b}, O. Bondarenko²², I. Boyko²¹, S. Braun³⁷, R. A. Briere⁴, H. Cai⁴⁷, X. Cai¹, O. Cakir^{36A}, A. Calcaterra^{19A}, G. F. Cao¹, S. A. Cetin^{36B}, J. F. Chang¹, G. Chelkov^{21,b}, G. Chen¹, H. S. Chen¹, J. C. Chen¹, M. L. Chen¹, S. J. Chen²⁶, X. Chen¹, X. R. Chen²³, Y. B. Chen¹, H. P. Cheng¹⁶, X. K. Chu²⁸, Y. P. Chu¹, D. Cronin-Hennessy⁴⁰, H. L. Dai¹, J. P. Dai¹, D. Dedovich²¹, Z. Y. Deng¹, A. Denig²⁰, I. Denysenko²¹, M. Destefanis^{45A,45C}, W. M. Ding³⁰, Y. Ding²⁴, C. Dong²⁷, J. Dong¹, L. Y. Dong¹, M. Y. Dong¹, S. X. Du⁴⁹, J. Z. Fan³⁵, J. Fang¹, S. S. Fang¹, Y. Fang¹, L. Fava^{45B,45C}, C. Q. Feng⁴², C. D. Fu¹, O. Fuks^{21,b}, Q. Gao¹, Y. Gao³⁵, C. Geng⁴², K. Goetzen⁹, W. X. Gong¹, W. Gradl²⁰, M. Greco^{45A,45C}, M. H. Gu¹, Y. T. Gu¹¹, Y. H. Guan¹, A. Q. Guo²⁷, L. B. Guo²⁵, T. Guo²⁵, Y. P. Guo²⁰, Y. L. Han¹, F. A. Harris³⁹, K. L. He¹, M. He¹, Z. Y. He²⁷, T. Held³, Y. K. Heng¹, Z. L. Hou¹, C. Hu²⁵, H. M. Hu¹, J. F. Hu³⁷, T. Hu¹, G. M. Huang⁵, G. S. Huang⁴², H. P. Huang⁴⁷, J. S. Huang¹⁴, L. Huang¹, X. T. Huang³⁰, Y. Huang²⁶, T. Hussain⁴⁴, C. S. Ji⁴², Q. Ji¹, Q. P. Ji²⁷, X. B. Ji¹, X. L. Ji¹, L. L. Jiang¹, L. W. Jiang⁴⁷, X. S. Jiang¹, J. B. Jiao³⁰, Z. Jiao¹⁶, D. P. Jin¹, S. Jin¹, T. Johansson⁴⁶, N. Kalantar-Nayestanaki²², X. L. Kang¹, X. S. Kang²⁷, M. Kavatsyuk²², B. Kloss²⁰, B. Kopf³, M. Kornicer³⁹, W. Kühn³⁷, A. Kupsc⁴⁶, W. Lai¹, J. S. Lange³⁷, M. Lara¹⁸, P. Larin¹³, M. Leyhe³, C. H. Li¹, Cheng Li⁴², Cui Li⁴², D. Li¹⁷, D. M. Li⁴⁹, F. Li¹, G. Li¹, H. B. Li¹, J. C. Li¹, K. Li³⁰, K. Li¹², Lei Li¹, P. R. Li³⁸, Q. J. Li¹, T. Li³⁰, W. D. Li¹, W. G. Li¹, X. L. Li³⁰, X. N. Li¹, X. Q. Li²⁷, Z. B. Li³⁴, H. Liang⁴², Y. F. Liang³², Y. T. Liang³⁷, D. X. Lin¹³, B. J. Liu¹, C. L. Liu⁴, C. X. Liu¹, F. H. Liu³¹, Fang Liu¹, Feng Liu⁵, H. B. Liu¹¹, H. H. Liu¹⁵, H. M. Liu¹, J. Liu¹, J. P. Liu⁴⁷, K. Liu³⁵, K. Y. Liu²⁴, P. L. Liu³⁰, Q. Liu³⁸, S. B. Liu⁴², X. Liu²³, Y. B. Liu²⁷, Z. A. Liu¹, Zhiqiang Liu¹, Zhiqing Liu²⁰, H. Loehner²², X. C. Lou^{1,c}, G. R. Lu¹⁴, H. J. Lu¹⁶, H. L. Lu¹, J. G. Lu¹, X. R. Lu³⁸, Y. Lu¹, Y. P. Lu¹, C. L. Luo²⁵, M. X. Luo⁴⁸, T. Luo³⁹, X. L. Luo¹, M. Lv¹, F. C. Ma²⁴, H. L. Ma¹, Q. M. Ma¹, S. Ma¹, T. Ma¹, X. Y. Ma¹, F. E. Maas¹³, M. Maggiora^{45A,45C}, Q. A. Malik⁴⁴, Y. J. Mao²⁸, Z. P. Mao¹, J. G. Messchendorp²², J. Min¹, T. J. Min¹, R. E. Mitchell¹⁸, X. H. Mo¹, Y. J. Mo⁵, H. Moeini²², C. Morales Morales¹³, K. Moriya¹⁸, N. Yu. Muchnoi^{8,a}, H. Muramatsu⁴⁰, Y. Nefedov²¹, I. B. Nikolaev^{8,a}, Z. Ning¹, S. Nisar⁷, X. Y. Niu¹, S. L. Olsen²⁹, Q. Ouyang¹, S. Pacetti^{19B}, M. Pelizaeus³, H. P. Peng⁴², K. Peters⁹, J. L. Ping²⁵, R. G. Ping¹, R. Poling⁴⁰, N. Q.⁴⁷, M. Qi²⁶, S. Qian¹, C. F. Qiao³⁸, L. Q. Qin³⁰, X. S. Qin¹, Y. Qin²⁸, Z. H. Qin¹, J. F. Qiu¹, K. H. Rashid⁴⁴, C. F. Redmer²⁰, M. Ripka²⁰, G. Rong¹, X. D. Ruan¹¹, A. Sarantsev^{21,d}, K. Schoenning⁴⁶, S. Schumann²⁰, W. Shan²⁸, M. Shao⁴², C. P. Shen², X. Y. Shen¹, H. Y. Sheng¹, M. R. Shepherd¹⁸, W. M. Song¹, X. Y. Song¹, S. Spataro^{45A,45C}, B. Spruck³⁷, G. X. Sun¹, J. F. Sun¹⁴, S. S. Sun¹, Y. J. Sun⁴², Y. Z. Sun¹, Z. J. Sun¹, Z. T. Sun⁴², C. J. Tang³², X. Tang¹, I. Tapan^{36C}, E. H. Thorndike⁴¹, D. Toth⁴⁰, M. Ullrich³⁷, I. Uman^{36B}, G. S. Varner³⁹, B. Wang²⁷, D. Wang²⁸, D. Y. Wang²⁸, K. Wang¹, L. L. Wang¹, L. S. Wang¹, M. Wang³⁰, P. Wang¹, P. L. Wang¹, Q. J. Wang¹, S. G. Wang²⁸, W. Wang¹, X. F. Wang³⁵, Y. D. Wang^{19A}, Y. F. Wang¹, Y. Q. Wang²⁰, Z. Wang¹, Z. G. Wang¹, Z. H. Wang⁴², Z. Y. Wang¹, D. H. Wei¹⁰, J. B. Wei²⁸, P. Weidenkaff²⁰, S. P. Wen¹, M. Werner³⁷, U. Wiedner³, M. Wolke⁴⁶, L. H. Wu¹, N. Wu¹, Z. Wu¹, L. G. Xia³⁵, Y. Xia¹⁷, D. Xiao¹, Z. J. Xiao²⁵, Y. G. Xie¹, Q. L. Xiu¹, G. F. Xu¹, L. Xu¹, Q. J. Xu¹², Q. N. Xu³⁸, X. P. Xu³³, Z. Xue¹, L. Yan⁴², W. B. Yan⁴², W. C. Yan⁴², Y. H. Yan¹⁷, H. X. Yang¹, L. Yang⁴⁷, Y. Yang⁵, Y. X. Yang¹⁰, H. Ye¹, M. Ye¹, M. H. Ye⁶, B. X. Yu¹, C. X. Yu²⁷, H. W. Yu²⁸, J. S. Yu²³, S. P. Yu³⁰, C. Z. Yuan¹, W. L. Yuan²⁶, Y. Yuan¹, A. Yuncu^{36B}, A. A. Zafar⁴⁴, A. Zallo^{19A}, S. L. Zang²⁶, Y. Zeng¹⁷, B. X. Zhang¹, B. Y. Zhang¹, C. Zhang²⁶, C. B. Zhang¹⁷, C. C. Zhang¹, D. H. Zhang¹, H. H. Zhang³⁴, H. Y. Zhang¹, J. J. Zhang¹, J. Q. Zhang¹, J. W. Zhang¹, J. Y. Zhang¹, J. Z. Zhang¹, S. H. Zhang¹, X. J. Zhang¹, X. Y. Zhang³⁰, Y. Zhang¹, Y. H. Zhang¹, Z. H. Zhang⁵, Z. P. Zhang⁴², Z. Y. Zhang⁴⁷, G. Zhao¹, J. W. Zhao¹, Lei Zhao⁴², Ling Zhao¹, M. G. Zhao²⁷, Q. Zhao¹, Q. W. Zhao¹, S. J. Zhao⁴⁹, T. C. Zhao¹, X. H. Zhao²⁶, Y. B. Zhao¹, Z. G. Zhao⁴², A. Zhemchugov^{21,b}, B. Zheng⁴³, J. P. Zheng¹, Y. H. Zheng³⁸, B. Zhong²⁵, L. Zhou¹, Li Zhou²⁷, X. Zhou⁴⁷, X. K. Zhou³⁸, X. R. Zhou⁴², X. Y. Zhou¹, K. Zhu¹, K. J. Zhu¹, X. L. Zhu³⁵, Y. C. Zhu⁴², Y. S. Zhu¹, Z. A. Zhu¹, J. Zhuang¹, B. S. Zou¹, J. H. Zou¹

(BESIII Collaboration)

¹ Institute of High Energy Physics, Beijing 100049, People's Republic of China

² Beihang University, Beijing 100191, People's Republic of China

³ Bochum Ruhr-University, D-44780 Bochum, Germany

⁴ Carnegie Mellon University, Pittsburgh, Pennsylvania 15213, USA

- ⁵ *Central China Normal University, Wuhan 430079, People's Republic of China*
- ⁶ *China Center of Advanced Science and Technology, Beijing 100190, People's Republic of China*
- ⁷ *COMSATS Institute of Information Technology, Lahore, Defence Road, Off Raiwind Road, 54000 Lahore*
- ⁸ *G.I. Budker Institute of Nuclear Physics SB RAS (BINP), Novosibirsk 630090, Russia*
- ⁹ *GSI Helmholtzcentre for Heavy Ion Research GmbH, D-64291 Darmstadt, Germany*
- ¹⁰ *Guangxi Normal University, Guilin 541004, People's Republic of China*
- ¹¹ *GuangXi University, Nanning 530004, People's Republic of China*
- ¹² *Hangzhou Normal University, Hangzhou 310036, People's Republic of China*
- ¹³ *Helmholtz Institute Mainz, Johann-Joachim-Becher-Weg 45, D-55099 Mainz, Germany*
- ¹⁴ *Henan Normal University, Xinxiang 453007, People's Republic of China*
- ¹⁵ *Henan University of Science and Technology, Luoyang 471003, People's Republic of China*
- ¹⁶ *Huangshan College, Huangshan 245000, People's Republic of China*
- ¹⁷ *Hunan University, Changsha 410082, People's Republic of China*
- ¹⁸ *Indiana University, Bloomington, Indiana 47405, USA*
- ¹⁹ *(A)INFN Laboratori Nazionali di Frascati, I-00044, Frascati, Italy; (B)INFN and University of Perugia, I-06100, Perugia, Italy*
- ²⁰ *Johannes Gutenberg University of Mainz, Johann-Joachim-Becher-Weg 45, D-55099 Mainz, Germany*
- ²¹ *Joint Institute for Nuclear Research, 141980 Dubna, Moscow region, Russia*
- ²² *KVI, University of Groningen, NL-9747 AA Groningen, The Netherlands*
- ²³ *Lanzhou University, Lanzhou 730000, People's Republic of China*
- ²⁴ *Liaoning University, Shenyang 110036, People's Republic of China*
- ²⁵ *Nanjing Normal University, Nanjing 210023, People's Republic of China*
- ²⁶ *Nanjing University, Nanjing 210093, People's Republic of China*
- ²⁷ *Nankai University, Tianjin 300071, People's Republic of China*
- ²⁸ *Peking University, Beijing 100871, People's Republic of China*
- ²⁹ *Seoul National University, Seoul, 151-747 Korea*
- ³⁰ *Shandong University, Jinan 250100, People's Republic of China*
- ³¹ *Shanxi University, Taiyuan 030006, People's Republic of China*
- ³² *Sichuan University, Chengdu 610064, People's Republic of China*
- ³³ *Soochow University, Suzhou 215006, People's Republic of China*
- ³⁴ *Sun Yat-Sen University, Guangzhou 510275, People's Republic of China*
- ³⁵ *Tsinghua University, Beijing 100084, People's Republic of China*
- ³⁶ *(A)Ankara University, Dogol Caddesi, 06100 Tandogan, Ankara, Turkey; (B)Dogus University, 34722 Istanbul, Turkey; (C)Uludag University, 16059 Bursa, Turkey*
- ³⁷ *Universitaet Giessen, D-35392 Giessen, Germany*
- ³⁸ *University of Chinese Academy of Sciences, Beijing 100049, People's Republic of China*
- ³⁹ *University of Hawaii, Honolulu, Hawaii 96822, USA*
- ⁴⁰ *University of Minnesota, Minneapolis, Minnesota 55455, USA*
- ⁴¹ *University of Rochester, Rochester, New York 14627, USA*
- ⁴² *University of Science and Technology of China, Hefei 230026, People's Republic of China*
- ⁴³ *University of South China, Hengyang 421001, People's Republic of China*
- ⁴⁴ *University of the Punjab, Lahore-54590, Pakistan*
- ⁴⁵ *(A)University of Turin, I-10125, Turin, Italy; (B)University of Eastern Piedmont, I-15121, Alessandria, Italy; (C)INFN, I-10125, Turin, Italy*
- ⁴⁶ *Uppsala University, Box 516, SE-75120 Uppsala*
- ⁴⁷ *Wuhan University, Wuhan 430072, People's Republic of China*
- ⁴⁸ *Zhejiang University, Hangzhou 310027, People's Republic of China*
- ⁴⁹ *Zhengzhou University, Zhengzhou 450001, People's Republic of China*
- ^a *Also at the Novosibirsk State University, Novosibirsk, 630090, Russia*
- ^b *Also at the Moscow Institute of Physics and Technology, Moscow 141700, Russia*
- ^c *Also at University of Texas at Dallas, Richardson, Texas 75083, USA*

^d Also at the PNPI, Gatchina 188300, Russia

(Dated: August 12, 2014)

The process $e^+e^- \rightarrow p\bar{p}\pi^0$ has been studied by analyzing data collected at $\sqrt{s} = 3.773$ GeV, at $\sqrt{s} = 3.650$ GeV, and during a $\psi(3770)$ line shape scan with the BESIII detector at the BEPCII collider. The Born cross section of $p\bar{p}\pi^0$ in the vicinity of the $\psi(3770)$ is measured and the Born cross section of $\psi(3770) \rightarrow p\bar{p}\pi^0$ is extracted considering interference between resonant and continuum production amplitudes. Two solutions with the same probability and a significance of 1.5σ are found. The solutions for the Born cross section of $\psi(3770) \rightarrow p\bar{p}\pi^0$ are $33.8 \pm 1.8 \pm 2.1$ pb and $0.06^{+0.10+0.01}_{-0.04-0.01}$ pb (< 0.22 pb at a 90% confidence level). Using the estimated cross section and a constant decay amplitude approximation, the cross section $\sigma(p\bar{p} \rightarrow \psi(3770)\pi^0)$ is calculated for the kinematic situation of the planned PANDA experiment. The maximum cross section corresponding to the two solutions is expected to be less than 0.79 nb at 90% confidence level and 122 ± 10 nb at a center of mass energy of 5.26 GeV.

PACS numbers: 13.66.BC, 13.25.Gv, 14.40.Lb, 14.20.Dh

INTRODUCTION

The PANDA (AntiProton Annihilations at Darmstadt) experiment to be built as a part of the future Facility for Antiproton and Ion Research (FAIR) located at Gesellschaft für Schwerionenforschung (GSI) facility in Darmstadt (Germany) will address aspects in the field of non-perturbative quantum chromodynamics [1]. The PANDA experiment is designed to exploit the physics potential arising from a cooled high-intensity antiproton beam covering the center of mass energy range between ~ 2.3 and 5.5 GeV and will perform studies of antiproton-proton annihilation and reactions of antiprotons with heavier nuclear targets [1]. The scientific program includes among other things the hadron spectroscopy up to the region of charm quarks and especially a detailed investigation of the spectrum of charmonium and charmonium hybrid states in the open charm sector, including the determination of masses, decay widths, decay properties and quantum numbers [1].

All neutral states with non-exotic quantum numbers J^{PC} can be directly produced in $p\bar{p}$ formation reactions. However, J^{PC} exotic states can be produced in association with a meson, e.g. an additional pion: $p\bar{p} \rightarrow \pi^0 X$, where X is a J^{PC} exotic hybrid or charmonium state [2]. To prepare experiments with PANDA, estimates for the production cross sections are required. They can be estimated by models relying on constant amplitude approximations and crossing symmetries requiring the a priori unknown $p\bar{p}\pi^0$ partial decay width of the states as an input parameter [2].

$p\bar{p}\pi^0$ decay widths for charmonium states below the open charm threshold have been reported by various experiments and are relatively well known [3]. However, information on the partial decay widths of higher lying charmonium states is still lacking [3].

The lightest charmonium state which can decay to $D\bar{D}$ pairs is the $\psi(3770)$ resonance. It was predicted

by Eichten *et al.* [4] and discovered by Rapidis *et al.* [5] and has a mass of (3773.15 ± 0.33) MeV/ c^2 and a width of (27.2 ± 1.0) MeV [3].

As the mass of the $\psi(3770)$ is slightly above the $D\bar{D}$ threshold and its width is large, it was expected to decay entirely into $D\bar{D}$ final states [6]. However, the BES collaboration measured the total non- $D\bar{D}$ branching fraction to be $(14.7 \pm 3.2)\%$ neglecting interference effects [7–10]. The CLEO collaboration measured the non- $D\bar{D}$ branching fraction to be $(-3.3 \pm 1.4^{+6.6}_{-4.8})\%$ taking into account interference between electromagnetic resonant and electromagnetic non-resonant (continuum) amplitude assuming no interference with the three-gluon amplitude [11]. The different results might be explained by different treatments of the interference between electromagnetic resonant and electromagnetic non-resonant (continuum) amplitude. Meanwhile it has also been noticed that the interference of the continuum amplitude with the 3-gluon resonant amplitude, which is dominant compared to the electromagnetic resonant amplitude in $\psi(3770)$ decays [12], should be taken into account as well [12, 13].

The decay channel of $\psi(3770) \rightarrow p\bar{p}$ has been studied recently by the BESIII collaboration considering interference between resonant and continuum amplitude [14]. The measured energy dependence of the cross section was found to be in agreement with destructive interference and two indistinguishable solutions for the cross section of $p\bar{p} \rightarrow \psi(3770)$ have been found, one of which is less than 27.5 nb at 90% confidence level and the other is $425.6^{+42.9}_{-43.7}$ nb.

In this paper, the Born cross section of $e^+e^- \rightarrow p\bar{p}\pi^0$ in the vicinity of the $\psi(3770)$ resonance is studied using data taken by the Beijing Spectrometer III (BESIII) experiment. The cross section of the decay $\psi(3770) \rightarrow p\bar{p}\pi^0$ is measured taking into account the interference between the continuum and resonant production amplitudes and the cross section of $p\bar{p} \rightarrow \psi(3770)\pi^0$, which is an estimate for open charm production in $p\bar{p}$ annihilations, for the kinematic situation at the PANDA experiment is

evaluated using a model based on a constant amplitude approximation [2].

EXPERIMENT AND DATA SAMPLES

The BESIII experiment is situated at the Beijing Electron-Positron Collider II (BEPCII) at the Institute of High Energy Physics (IHEP). BEPCII and BESIII [15] are major upgrades of the BESII experiment and the BEPC collider [16]. They cover the energy range from about $\sqrt{s} = 2$ GeV up to 4.6 GeV and thus allow for the study of physics in the τ -charm energy region. The double-ring e^+e^- collider is designed for a peak luminosity of $10^{33} \text{ cm}^{-2}\text{s}^{-1}$ at a beam current of 0.93 A at the $\psi(3770)$ resonance peak. The detector, with an angular acceptance of about 93% of 4π , consists of 5 major components: (1) The innermost component is a helium gas based Main Drift Chamber (MDC), which has in total 43 layers, providing a single wire spatial resolution of 135 micron, a dE/dx resolution of better than 6%, and a momentum resolution of $\sim 0.5\%$ for charged particles with momenta of 1 GeV/c in a 1 Tesla magnetic field. (2) The Time of Flight (TOF) system for particle identification (PID) is composed of a two-layer structure in the barrel and a one layer structure in the endcap region. It is built of plastic scintillators and provides a time resolution of 80 ps (110 ps) in the barrel (endcap) system, allowing a pion/kaon separation at a 95% confidence level (C.L.) up to about 1 GeV/c. (3) The Electromagnetic Calorimeter (EMC), which surrounds the MDC and the TOF system, consists of 6240 thallium doped cesium-iodide crystals and provides an energy resolution of 2.5% (5.0%) and a position resolution of 6 mm (9 mm) for photons with an energy of 1 GeV in the barrel (endcaps) part. (4) The superconducting solenoid magnet surrounds these three inner components, providing an axial uniform magnetic field of 1.0 Tesla. (5) The muon chamber system, embedded in the flux return of the magnet, consists of 9 (8) layers of Resistive Plate Chambers (RPCs) in the barrel (endcap) region and provides a spatial resolution of 2 cm.

This paper presents a study of $e^+e^- \rightarrow p\bar{p}\pi^0$, which uses the following data sets collected with the BESIII detector: A data set ($\mathcal{L} = 2.9 \text{ fb}^{-1}$) collected at the peak position of the $\psi(3770)$ resonance (3.773 GeV/c²) [17], a data set ($\mathcal{L} = 44 \text{ pb}^{-1}$) collected at a center of mass energy of 3.650 GeV [17], and 60 pb⁻¹ of data accumulated during a $\psi(3770)$ line-shape scan. For the sake of statistics, 25 small data sets in the scan data with varying luminosities in the energy range from 3.736 GeV to 3.813 GeV have been merged together into 7 separate data sets. The resulting center of mass energies of each set have been calculated by weighting the center of mass energies of the small data sets with their luminosity. Errors arising from this merging are considered in the systematic error (see section "Systematics Errors").

A Geant4-based [18] Monte Carlo (MC) simulation software taking into account the geometric and material description of the BESIII detector and the detector response is used for the determination of the detection efficiencies, the optimization of event selection criteria and the estimation of backgrounds. Since the intermediate products of the decay $\psi(3770) \rightarrow p\bar{p}\pi^0$ (e.g. nucleon resonances) are unknown, the detection efficiency has been determined taking into account the kinematic properties of the decay products at different position in the Dalitz plot using simulated MC events. Polarization effects of the intermediate states, which might affect the detection efficiencies, are taken into account, too. Therefore, the extracted distribution of the polar angle of the π^0 in the data, which deviates from a phase space distribution, has been fitted and is taken as input in the simulation of MC samples (compare to figure 1).

Initial State Radiation (ISR) effects are not considered in the determination of the detection efficiencies, but are taken into account later. For the estimation of background contributions from $\gamma_{\text{ISR}}J/\psi$, $\gamma_{\text{ISR}}\psi(3686)$ and $e^+e^- \rightarrow \psi(3770) \rightarrow D\bar{D}$ samples of MC events with a size equivalent to 1.3 and 4.8 times of the collected data are analyzed, respectively. Background arising from exclusive processes similar to the analyzed one, for example decays into $p\bar{p}\pi^0\gamma$, are investigated with MC samples containing 20,000 events of the respective process each.

EVENT SELECTION

For $e^+e^- \rightarrow p\bar{p}\pi^0$ events, the π^0 candidates are reconstructed by their dominant decay channel into two photons, resulting in a final state with two oppositely charged particles and two neutral photons. Hence, events with two charged particles resulting in a net charge of zero and at least two photon candidates are selected. The polar angles of charged tracks in the MDC have to satisfy $|\cos\theta| < 0.93$, and the point of closest approach with respect to the e^+e^- interaction point is required to be within ± 10 cm in the beam direction and ± 1 cm in the plane perpendicular to the beam axis. The combined information of the specific energy loss of a particle in the MDC (dE/dx) and its TOF is used to calculate for each charged particle the confidence level for being a pion, a kaon or a proton/antiproton. A proton/antiproton candidate has to satisfy $CL_p > CL_\pi$ and $CL_p > CL_K$, where CL_x stands for the respective confidence level of the particle being a proton/antiproton, pion or kaon. Due to differences in detection efficiencies between data and MC simulations for small transverse momenta, the proton/antiproton candidates are required to have transverse momenta larger than 300 MeV/c.

Photon candidates are reconstructed by their energy deposition in the EMC and are required to deposit at least 25 MeV in the barrel region ($|\cos\theta| < 0.8$) and

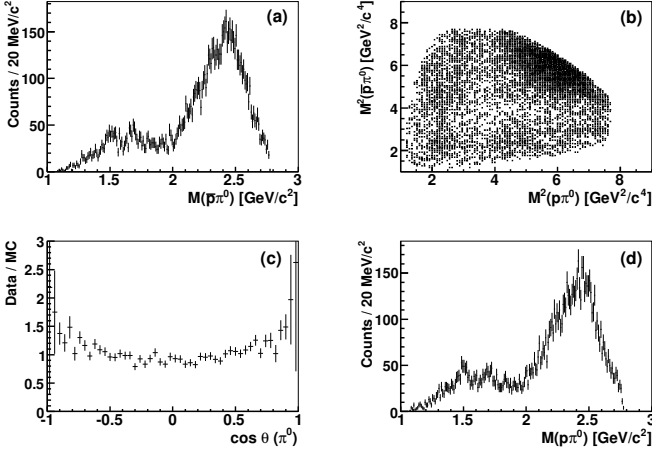


Figure 1. (a): Distribution of the invariant mass $M(\bar{p}\pi^0)$; (b): Dalitz plot of $M^2(p\pi^0)$ vs. $M^2(\bar{p}\pi^0)$; (c): ratio of data and phase-space distributed signal MC for $\cos\theta$ of π^0 candidates; and (d): invariant mass $M(p\pi^0)$, of all candidate events passing the event selection.

50 MeV in the endcaps ($0.86 < \cos\theta < 0.92$). Showers from charged particles in the EMC are suppressed by requiring the angle between a photon candidate and a proton to be larger than 10° and between a photon candidate and an antiproton to be larger than 30° .

Events with a proton, an antiproton, and at least two photons are subjected to a five-constraint (5C) kinematic fit to the initial 4-momentum of the colliding electrons and positrons and to the π^0 mass of the two photons, to provide more accurate momentum information on the final state. The χ^2 of the kinematic fit is required to be less than 50 and π^0 candidates are required to be within a $\pm 3\sigma$ region of the π^0 mass to further reduce background. When more than two photon candidates are found, all possible $p\bar{p}\gamma\gamma$ combinations are considered and the one resulting in the smallest χ^2 is selected for further analysis. Figure 1 shows the Dalitz plot and the projections of the Dalitz plot for all events selected at an energy of 3.773 GeV.

BACKGROUND ESTIMATION

Background from radiative return to the lower lying $J^{PC} = 1^{--}$ $\psi(3686)$ and J/ψ resonances, which is not considered in the ISR correction procedure, has been estimated using inclusive MC samples. This ISR related background is determined to be smaller than 0.5% and its contribution will be considered in the cross section calculation. Contributions from $\gamma_{\text{ISR}}J/\psi$ arise mainly due to reconstruction of fake π^0 s with the radiated ISR photons. Background from $D\bar{D}$ decays at an energy of 3.773 GeV is also estimated using inclusive MC samples. It is on the order of 0.015% of all reconstructed events and thus has been neglected. The data taken at 3.650 GeV can

contain contributions from the $\psi(3686)$ tail. Its cross section is estimated in [19] to be 0.136 ± 0.012 nb and this $\psi(3686)$ tail contribution is also considered in the cross section calculation. The contributions of other decay channels ($\psi(3770) \rightarrow \gamma\chi_{ci} \rightarrow \gamma p\bar{p}(\pi^0)$ where $i = 0, 1, 2$, $\psi(3770) \rightarrow \gamma\eta_c \rightarrow \gamma p\bar{p}$, $\psi(3770) \rightarrow \gamma\eta_c(2S) \rightarrow \gamma p\bar{p}$, $\psi(3770) \rightarrow p\bar{p}$, $\psi(3770) \rightarrow p\bar{p}\gamma$, $\psi(3770) \rightarrow p\bar{p}\pi^0\gamma$, $\psi(3770) \rightarrow p\bar{p}\pi^0\gamma\gamma$) were estimated to be less than 0.4% of all reconstructed events at each analyzed energy point. The contributions of decay channels with yet unmeasured branching ratios for the $\psi(3770)$ resonance have been estimated by the corresponding decay channels of $\psi(3686)$ and by π^0 sideband estimations and their number cannot be simply subtracted and will be considered in the systematic error.

CALCULATION OF THE CROSS SECTIONS

The observed cross sections at $\sqrt{s}=3.650$ GeV and eight more energy points in the range from 3.746 GeV up to 3.804 GeV, including the data collected at the peak of $\psi(3770)$ have been calculated according to $\sigma_{\text{obs.}} = \frac{N_{\text{sig.}}}{\epsilon\mathcal{L}}$, where \mathcal{L} is the integrated luminosity, ϵ the corresponding detection efficiency (which includes also the branching fraction of the π^0 into two photons from [3]) and $N_{\text{sig.}}$ the number of events passing the event selection. The background contribution from radiative returns to the lower lying $J^{PC} = 1^{--}$ $\psi(3686)$ and J/ψ resonances has been subtracted from $N_{\text{sig.}}$.

The observed cross section is related to the Born cross section by $\sigma_0 = \sigma_{\text{obs.}}/(1 + \delta)$, with σ_0 the Born cross section, $\sigma_{\text{obs.}}$ the observed cross section and $1 + \delta$ the radiative correction factor, which includes ISR contributions, vertex corrections, and terms arising from the e^+e^- self-energy and the hadronic and leptonic vacuum polarization. The factor $1 + \delta$ is calculated with the method described in [20, 21]. The contributions from vertex corrections, e^+e^- self-energy and the hadronic and leptonic vacuum polarization are independent from the lineshape of the cross section, but not the ISR contribution. As input for the lineshape a fit of equation 1 to the observed cross sections $\sigma_{\text{obs.}}$ is used and the radiative correction factors are calculated. The cross sections are then refined iteratively. At each iteration, the radiative correction factors are calculated and the cross sections are updated accordingly. After the first iteration, the radiative correction factors change by less than 10%, after the second iteration by less than 2%. After the sixth iteration the radiative correction factors remain constant. The maximum energy for the ISR photons considered in the radiative correction procedure is 9% of the beam energy. Table I gives an overview of the reconstructed events, determined cross sections, radiative correction factors and calculated Born cross sections. Figure 2 shows the calculated Born cross sections of $e^+e^- \rightarrow p\bar{p}\pi^0$ for the inves-

Table I. Summary of measurements of the number of reconstructed decays into $p\bar{p}\pi^0$ (before applying any corrections), the luminosities \mathcal{L} , the average reconstruction efficiency $\epsilon_{\text{average}}$ (reconstructed counts divided by efficiency corrected counts), the observed cross sections $\sigma_{\text{obs.}}$, the radiative correction factors $1+\delta$ and the calculated Born cross sections σ_0 . The small efficiency at 3.780 GeV is due to the observed event distribution in the Dalitz plot. The first error is the statistical error, the second one the *uncorrelated* systematic uncertainty. Correlated systematic uncertainties are not considered here.

Energy [GeV]	Counts	\mathcal{L} [pb $^{-1}$]	$\epsilon_{\text{average}}$ [%]	$\sigma_{\text{obs.}}^{e^+e^- \rightarrow p\bar{p}\pi^0}$ [pb]	$1+\delta$	$\sigma_0^{e^+e^- \rightarrow p\bar{p}\pi^0}$ [pb]
3.650	165 ± 12.8	$44.49 \pm 0.02 \pm 0.44$	$43.9 \pm 0.1 \pm 1.5$	$8.44 \pm 0.69 \pm 0.14$	0.84	$10.09 \pm 0.84 \pm 0.16$
3.746	$19^{+4.8}_{-4.2}$	$4.94 \pm 0.01 \pm 0.05$	$45.5 \pm 0.1 \pm 1.5$	$8.46^{+2.16}_{-1.87} \pm 0.14$	0.88	$9.60^{+2.45}_{-2.12} \pm 0.16$
3.753	28 ± 5.3	$9.31 \pm 0.02 \pm 0.10$	$47.0 \pm 0.1 \pm 1.5$	$6.40 \pm 1.22 \pm 0.10$	0.88	$7.28 \pm 1.38 \pm 0.12$
3.757	35 ± 5.9	$8.04 \pm 0.01 \pm 0.09$	$47.2 \pm 0.1 \pm 1.5$	$9.22 \pm 1.57 \pm 0.15$	0.88	$10.44 \pm 1.77 \pm 0.17$
3.765	42 ± 6.5	$11.86 \pm 0.02 \pm 0.13$	$45.9 \pm 0.1 \pm 1.5$	$7.72 \pm 1.20 \pm 0.12$	0.88	$8.73 \pm 1.35 \pm 0.14$
3.773	9107 ± 95.4	$2916.94 \pm 0.18 \pm 29.17$	$45.5 \pm 0.1 \pm 1.5$	$6.83 \pm 0.08 \pm 0.11$	0.89	$7.71 \pm 0.09 \pm 0.13$
3.780	$13^{+4.3}_{-3.7}$	$5.70 \pm 0.01 \pm 0.06$	$32.7 \pm 0.1 \pm 1.5$	$6.98^{+2.34}_{-2.03} \pm 0.11$	0.88	$7.92^{+2.66}_{-2.31} \pm 0.13$
3.791	45 ± 6.7	$12.45 \pm 0.02 \pm 0.07$	$45.8 \pm 0.1 \pm 1.5$	$7.87 \pm 1.18 \pm 0.13$	0.87	$9.03 \pm 1.35 \pm 0.15$
3.804	33 ± 5.8	$10.15 \pm 0.03 \pm 0.06$	$44.2 \pm 0.1 \pm 1.5$	$7.37 \pm 1.29 \pm 0.12$	0.87	$8.44 \pm 1.48 \pm 0.14$

tigated energy points.

SYSTEMATIC ERRORS

Uncorrelated systematic errors in the cross section measurement do not only arise from the aforementioned decay channels (0.4%, compare to section “Background Estimation”), but also from the size of the MC samples (0.5%) and the efficiency determination. The error on the efficiency has been determined to be smaller than 1.5% by comparing different parametrizations of the Dalitz plot (dividing it into 11×11 , 22×22 and 44×44 bins, respectively) for simulated MC events. These three error sources will be directly considered in the fit to the cross sections (compare to the next section).

The dominating systematic error sources are correlated among the different energy points and thus can not be considered directly in the fit — their effect on the final results is estimated by the *offset method* [22]. The largest correlated systematic error arises from the radiative correction procedure and the extraction of the Born cross section. It has been determined by comparing the applied radiative correction procedure with the structure function method proposed by [23] (2%), by a comparison of different MC decay models (3%) and by taking the largest difference of the results for different cuts (1.5%). To take into account polarization effects of intermediate states in the decay, the polar angle of the π^0 has been extracted by a fit from data. The systematic error for this procedure is determined by shifting the extracted values from the fit according to their error and calculating the cross sections again. The largest difference observed for the cross section is 0.7% and is taken as the systematic uncertainty.

The error which arises from the finite acceptance of the Dalitz plot at values larger than $7.7 \text{ GeV}^2/c^4$ on both axes is estimated to be smaller than 2%.

The error from the kinematic fit is due to inconsistencies of the MC simulation and data. It is estimated to be less than 2% by comparing an inclusive MC event sample and a selected control sample of data. Further errors arise from the MDC tracking efficiency (1% (p), 1% (\bar{p})), the particle identification (1% (p), 2% (\bar{p})), the photon detection efficiency (2%) [24] and the error on the center of mass energy measurement of less than 1 MeV. The integrated luminosity for the data taken at 3.65 GeV and 3.773 GeV was measured using large-angle Bhabha events, and has an estimated total uncertainty of 1.1% [17]. The luminosity of the line shape scan data is determined with large angle Bhabha events, too. The estimated uncertainty is also 1.1%.

The total systematic uncertainty of the individual energy points is calculated by adding the errors in quadrature and thus is 6.2%.

To estimate the error of the fit to the Born cross sections (see section “Fit to the Born Cross Sections”), which arises from the binning of the scan data points, two different sets of binning have been compared to the nominal one. The largest differences of the central values of the fit are taken as a systematic error and are added in quadrature to the systematic error of the fit results. The largest differences are 16% (*solution 1*) and 0.7% (*solution 2*) for the Born cross section $\sigma_0(\psi(3770) \rightarrow p\bar{p}\pi^0)$, and 3.7% (*solution 1*) and 0.1% (*solution 2*) for the phase ϕ .

FIT TO THE BORN CROSS SECTIONS

The cross section of the $\psi(3770)$ decay to $p\bar{p}\pi^0$ and other relevant quantities are extracted by a fit of

$$\sigma(s) = \left| \sqrt{\sigma_{\text{con}}} + \sqrt{\sigma_{\psi}} \frac{m\Gamma}{s-m^2+im\Gamma} \exp(i\phi) \right|^2 \quad (1)$$

to the calculated cross sections. The resonant production amplitude is usually composed of the electromag-

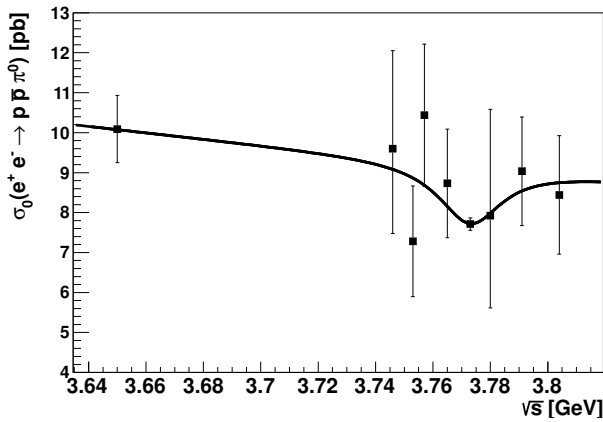


Figure 2. The calculated Born cross sections in e^+e^- annihilation to $p\bar{p}\pi^0$ at different energy points and the solution of the fitting procedure. The curve of both fit solutions is identical.

netic amplitude and the three-gluon amplitude. However, the electromagnetic amplitude can be neglected for the $\psi(3770)$ [12] and thus the resonant production amplitude can be described by $\sqrt{\sigma_\psi}$. The mass m and the width Γ of the $\psi(3770)$ have been fixed according to the world average values [3]. The continuum amplitude $\sqrt{\sigma_{con}}$ can be described by a function of s ; $\sigma_{con} = C/s^\lambda$, where the exponent λ is a priori unknown. The parameter ϕ describes the phase for an interference of resonant and continuum production amplitudes.

The continuum cross section itself is composed of two different components — an isospin $I = 0$ and an isospin $I = 1$ component — as the virtual photon arising as an intermediate state in an electron-positron annihilation can be associated with an isospin of $I = 0$ or $I = 1$. The ratio of the different isospin components of the virtual photon is for example discussed in [25, 26]. The basic idea is the dominance of single states in the virtual intermediate state, which can be for example (excited) ρ^* or ω^* mesons or coherent pion configurations with $I = 0$ and $I = 1$, resulting in a ratio of $(I=0) : (I=1) = 1 : 9$. Clearest evidence for such a ratio comes from the process $e^+e^- \rightarrow n\pi$ around 2 GeV, where the ratio of $I = 0$ and $I = 1$ is measured to be $\sim 1:9$ [25]. Also the electromagnetic decay width Γ_{ee} of the $\rho(770)$ and $\omega(782)$ mesons are in agreement with this ratio [3]. A constant ratio at higher energies is also consistent with the ideas of generalized vector meson dominance [25].

Hence, the continuum amplitude should be expressed as $A_{con} = A_{con}^{I=0} \exp(i\phi_1) + A_{con}^{I=1} \exp(i\phi_2)$ and Eq. 1 should contain two different phases. However, they can be combined again as a relative phase and one ends up with Eq. 1 considering the interference of the total continuum and resonant amplitudes.

The maximum likelihood fit yields two different solutions with the same $\chi^2/ndf = 2.70/5$ and thus with the same probability. A detailed explanation and a

mathematical review of the multiple solution problem is given in [27]. The solutions for the Born cross section $\sigma_0(\psi(3770) \rightarrow p\bar{p}\pi^0)$ are $0.06^{+0.10}_{-0.04}$ pb (*solution 1*) and 33.8 ± 1.8 pb (*solution 2*), respectively.

The results for the phases between resonant and continuum production amplitudes are $\phi = 269.8^{+52.4}_{-48.0}$ ° (*solution 1*) and $\phi = 269.7 \pm 2.3$ ° (*solution 2*), which both are in agreement with a destructive interference ($\simeq 270^\circ$). The parameters describing the slope of the continuum cross section are $C = (0.4 \pm 0.1) \cdot 10^3 \text{ GeV}^{2\lambda} \text{ pb}$ (*solution 1*), $C = (0.4 \pm 0.6) \cdot 10^3 \text{ GeV}^{2\lambda} \text{ pb}$ (*solution 2*) and $\lambda = 1.4 \pm 0.1$ (*solution 1*) and $\lambda = 1.4 \pm 0.6$ (*solution 2*). The unit and the large error of C are arising from the correlation of C and λ . The fit is shown in Figure 2. The statistical significance of the resonant amplitude, calculated based on the differences of the likelihood values between the fit with and without assuming a resonant contribution, is for both solutions 1.5σ .

Using the estimated cross section and the Born cross section of the $\psi(3770)$ resonance as given in [24], the cross section of the processes $p\bar{p} \rightarrow \psi(3770)\pi^0$ can be calculated based on a constant decay amplitude approximation [2] for the kinematic situation at the PANDA experiment. According to this model the maximum cross section can be expected at a center of mass energy of 5.26 GeV, which is still in reach of PANDA [1]; the results are < 0.79 nb at a 90% confidence level (*solution 1*) and 122 ± 10 nb (*solution 2*). The error for *solution 2* has been determined by taking the difference of the original solution and the solution using the sum of measured value and error as input value for the calculation.

Table II shows a compilation of the obtained results. Here, the systematic errors are considered. The upper limits at 90% C.L. are given for parameters where the error is dominating the measurement. The upper limits have been calculated assuming that the statistical and systematic errors are following a bifurcated Gaussian distribution.

SUMMARY

Using 2.9 fb^{-1} of data collected at $\sqrt{s} = 3.773 \text{ GeV}$, 44 pb^{-1} of data collected at $\sqrt{s} = 3.650 \text{ GeV}$ and 60 pb^{-1} of data collected during a $\psi(3770)$ line shape scan with the BESIII detector at the BEPCII collider, an analysis of the process $e^+e^- \rightarrow p\bar{p}\pi^0$ has been performed. The Born cross section of $e^+e^- \rightarrow \psi(3770) \rightarrow p\bar{p}\pi^0$ has been extracted allowing the continuum production amplitude to interfere with the resonant production amplitude. Two solutions with the same probability are found. The Born cross section is determined to be $0.06^{+0.10+0.01}_{-0.04-0.01}$ pb (< 0.22 pb at a 90% C.L.) or $33.8 \pm 1.8 \pm 2.1$ pb. Both phases of the fit solution are consistent with 270° , which is in agreement with a destructive interference. Using a constant decay amplitude approximation, the cross sec-

Table II. A summary of the extracted results from the fit. The upper limits are determined at a 90% C.L., where the first error given is from the fit (i.e. from the uncorrelated sources) and the second error is from the correlated systematics. The phases given are the one from the solutions of the fitting procedure.

Solution	$\sigma_0^{\psi(3770) \rightarrow p\bar{p}\pi^0}$ [pb]	ϕ_{Fit} [°]	$\sigma_0^{p\bar{p} \rightarrow \psi(3770)\pi^0}$ [nb] at 5.26 GeV
(1)	< 0.22	$269.8^{+52.4}_{-48.0} \pm 11.0$	< 0.79
(2)	$33.8 \pm 1.8 \pm 2.1$	$269.7 \pm 2.3 \pm 0.3$	122 ± 10

tions of $p\bar{p} \rightarrow \psi(3770)\pi^0$ are calculated to be less than 0.79 nb at a 90% C.L. and 122 ± 10 nb at center of mass energy of 5.26 GeV [2], respectively.

ACKNOWLEDGEMENT

The BESIII collaboration thanks the staff of BEPCII and the computing center for their strong support. This work is supported in part by the Ministry of Science and Technology of China under Contract No. 2009CB825200; Joint Funds of the National Natural Science Foundation of China under Contracts Nos. 11079008, 11179007, U1332201; National Natural Science Foundation of China (NSFC) under Contracts Nos. 10625524, 10821063, 10825524, 10835001, 10935007, 11125525, 11235011; the Chinese Academy of Sciences (CAS) Large-Scale Scientific Facility Program; CAS under Contracts Nos. KJCX2-YW-N29, KJCX2-YW-N45; 100 Talents Program of CAS; German Research Foundation DFG under Contract No. Collaborative Research Center CRC-1044; Istituto Nazionale di Fisica Nucleare, Italy; Ministry of Development of Turkey under Contract No. DPT2006K-120470; U. S. Department of Energy under Contracts Nos. DE-FG02-04ER41291, DE-FG02-05ER41374, DE-FG02-94ER40823, DESC0010118; U.S. National Science Foundation; University of Groningen (RuG) and the Helmholtzzentrum fuer Schwerionenforschung GmbH (GSI), Darmstadt; WCU Program of National Research Foundation of Korea under Contract No. R32-2008-000-10155-0.

- [1] M. Lutz *et al.* (PANDA Collaboration) arXiv:0903.3905 [hep-ex]
- [2] A. Lundborg, T. Barnes, and U. Wiedner, Phys. Rev. D **73**, 096003 (2006)
- [3] J. Beringer *et al.* (Particle Data Group), Phys. Rev. D **86**, 010001 (2012)
- [4] E. Eichten *et al.*, Phys. Rev. Lett. **34**, 369 (1975)
- [5] P. A. Rapidis *et al.*, Phys. Rev. Lett. **39**, 526 (1977)
- [6] W. Bacino *et al.*, Phys. Rev. Lett. **40**, 671 (1978)
- [7] M. Ablikim *et al.* (BES Collaboration), Phys. Lett. B **641**, 145 (2006)
- [8] M. Ablikim *et al.* (BES Collaboration), Phys. Rev. Lett. **97**, 121801 (2006)
- [9] M. Ablikim *et al.* (BES Collaboration), Phys. Lett. B **659**, 74 (2008)
- [10] M. Ablikim *et al.* (BES Collaboration), Phys. Rev. D **76**, 122002 (2007)
- [11] D. Besson *et al.* (CLEO Collaboration), Phys. Rev. Lett. **96**, 092002 (2006)
- [12] P. Wang, X. H. Mo, and C. Z. Yuan, International Journal of Modern Physics A **21**, 5163 (2006)
- [13] P. Wang, C. Yuan, X. Mo, and D. Zhang arXiv:hep-ph/0212139 [hep-ph]
- [14] M. Ablikim *et al.* (BESIII Collaboration), accepted by Phys. Lett. **B** (2014), arXiv:1403.6011 [hep-ex]
- [15] M. Ablikim *et al.* (BESIII Collaboration), Nucl. Instrum. Meth. A. **614**, 345 (2010)
- [16] J. Bai *et al.* (BES Collaboration), Nucl. Instrum. Meth. A. **344**, 319 (1994)
- [17] M. Ablikim *et al.* (BESIII Collaboration) arXiv:1307.2022 [hep-ex]
- [18] S. Agostinelli *et al.*, Nucl. Instrum. Meth. A. **506**, 250 (2003)
- [19] M. Ablikim *et al.* (BES Collaboration), Phys. Rev. D **76**, 122002 (2007)
- [20] H. Hu, X. Qi, G. Huang, and Z. Zhao, High Energy Physics and Nuclear Physics **25**, 701 (2001)
- [21] C. Edwards *et al.* (Crystall Ball Collaboration) SLAC-PUB-5160
- [22] M. Botje, Journal of Physics G: Nuclear and Particle Physics **28**, 779 (2002)
- [23] E. A. Kuraev and V. S. Fadin, Sov. J. Nucl. Phys **41**, 779 (1985)
- [24] M. Ablikim *et al.* (BESIII Collaboration), Phys. Rev. D **87**, 112011 (2013)
- [25] J. Ellis and M. Karliner, New Journal of Physics **4**, 18 (2002)
- [26] J. L. Rosner, Annals of Physics **319**, 1 (2005)
- [27] K. Zhu, X. H. Mo, C. Z. Yuan, and P. Wang, International Journal of Modern Physics A **26**, 4511 (2011)